For submission to BioRxiv

Evolution of gastrulation in cavefish: heterochronic cell movements and maternal factors

Jorge Torres-Paz, Julien Leclercq and Sylvie Rétaux*

Paris-Saclay Institute of Neuroscience, CNRS UMR9197, Université Paris-Sud and Université Paris-Saclay, Gif-sur-Yvette, France.

*Author for correspondence:

retaux@inaf.cnrs-gif.fr

Key words: *Astyanax mexicanus*, developmental evolution, heterochrony, dkk1b, prechordal plate, notochord

Summary

In animals the basic body plan is determined at early stages of embryogenesis. In fish and amphibians dorso-ventral polarity is established by maternal factors present in the oocyte. Downstream to the dorsalizing effect of maternal factors and the establishment of the organizer, the antero-posterior axis is specified during gastrulation, leading to the induction and regionalization of the neural tube. Subtle modifications in such early events are susceptible to have a major impact in later morphogenesis that can be deleterious or bring along morphological diversification. Here we used cave and surface morphotypes of the fish *Astyanax mexicanus* to study early embryonic events that could account for phenotypic evolution. First, we found differences in patterns, levels and dynamics of *dkk1b* expression in the prechordal plate from early gastrulation to somitogenesis. Our analyses of axial and paraxial mesodermal markers indicate that those differences might stem from heterochronic hypoblast internalization and convergent extension movements, which occur earlier in cavefish. Using F1 hybrid embryos obtained by reciprocal crosses of the two inter-fertile morphotypes we found that observed gastrulation differences depend fully on the maternal contribution. Later phenotypic differences in neural development became progressively hidden when zygotic genes take the control over development. Our work strongly suggests that maternal effect genes and developmental heterochronies occurring during gastrulation have impacted morphological brain change during cavefish evolution.

Introduction

Gastrulation is a fundamental process in organism development, leading to the establishment of the embryonic germ layers (endoderm, mesoderm and ectoderm) and the basic organization of the body plan. Although in vertebrates early embryonic development has adopted highly diverse configurations, gastrulation proceeds through evolutionary conserved morphogenetic movements, including the spreading of blastoderm cells (epiboly), the internalization of mesoderm and endoderm, convergent movements towards the prospective dorsal side and extension along the antero-posterior axis (convergence and extension, respectively) (Solnica-Krezel, 2005). Internalization of mesendodermal cells takes place through the blastopore, structurally circumferential in anamniotes (fishes and amphibians) and lineal in avian and mammalian amniotes (primitive streak).

A critical step for gastrulation to proceed is the establishment of the embryonic organizer (Spemann-Mangold organizer in frogs, shield in fishes, Hensen's node in birds and node in mammals), a signaling center essential to instruct the formation of the body axis. In fishes and amphibians the induction of the embryonic organizer in the prospective dorsal side occurs downstream to earlier developmental events, driven by maternal determinants deposited in the oocyte during maturation in the ovaries (Kelly et al., 2000; Nojima et al., 2004; Zhang et al., 1998). From the organizer will emerge the axial mesoderm, a structure that spans the complete rostro-caudal extent of the embryo, with the prechordal plate anteriorly and the notochord posteriorly. The axial mesoderm is the signaling center that will induce vertically the neural plate/tube in the overlying ectoderm.

The prechordal plate is key for the patterning of the forebrain, through the regulated secretion of morphogens including sonic hedgehog (shh), Fibroblast growth factors (fgf), and inhibitors of the Wingless-Int (WNT) pathway like dickkopf1b (dkk1b) and frizzled-related protein (frzb). Along its rostral migration, the prechordal plate is required for sequential patterning of forebrain elements (García-Calero et al., 2008; Puelles & Rubenstein, 2015), demonstrating a temporal and spatial requirement of this migratory cell population for brain development from gastrulation onwards.

Within the central nervous system, the forebrain plays a key role in processing sensory information coming from the environment and controlling higher cognitive functions. During evolution and across species, different forebrain modules have experienced impressive morphological modifications according to ecological needs, however the basic *Bauplan* to build the forebrain has been conserved. Temporal (heterochronic) and spatial (heterotopic) variation in the expression of regionalization genes and morphogens during embryogenesis have sculpted brain shapes along phylogeny.

An emergent model organism to study the impact of early embryogenesis on brain evolution at the microevolutionary scale is the characid fish *Astyanax mexicanus*. *A. mexicanus* species exists in two different eco-morphotypes distributed in Central and North America: a "wild type" river-dwelling fish (surface fish) and several geographically-isolated troglomorphic populations (cavefish), living in total and permanent darkness (Mitchell et al., 1977; Elliott, 2018). Fish from the cave morphotype can be easily identified because they lack eyes and pigmentation. As a result of the absence of visual information the cavefish has evolved mechanisms of sensory compensation, as enhanced olfactory and mechanosensory sensibilities (Hinaux et al., 2016; Yoshizawa et al, 2010). Sensory and other behavioral adaptations may have allowed them to increase the chances of finding food and mates in caves. Such behavioral changes are associated with morphological modifications such as larger olfactory sensory organs (Blin et al., 2018; Hinaux et al., 2016), increased number of facial mechanosensory neuromasts (Yoshizawa et al., 2014) and taste buds (Varatharasan et al., 2009), and modified serotonergic and orexinergic neurotransmission systems (Alié et al., 2018; Elipot et al., 2014; Jaggard et al., 2018). Remarkably, such morphological and behavioral adaptations have a developmental origin, mainly due to heterotopic and heterochronic differences in the expression of signaling molecules from midline organizers at the end of gastrulation, at the "neural plate" or bud stage. Subtle differences in *shh* and *fgf8* expression domains, larger and earlier respectively in cavefish compared to surface fish, affect downstream processes of gene expression, morphogenetic movements during neurulation and cell differentiation, driving the developmental evolution of cavefish nervous system (Hinaux et al., 2016; Menuet et al., 2007; Pottin et al., 2011; Ren et al., 2018; Yamamoto et al, 2004). These differences in genes expressed in the midline being already manifest in embryos at the end of body axis formation, we postulated they should stem from earlier developmental events during axis formation and gastrulation.

In order to search for variations in precocious ontogenetic programs leading to phenotypic evolution observed in *A. mexicanus* morphotypes, here we performed a systematic comparison of the gastrulation process in cave and surface embryos. We found that in the cavefish, the internalization of different mesodermal cell populations is more precocious, prompting us to go further backwards in embryogenesis and to investigate maternal components. Taking advantage of the inter-fertility of *A. mexicanus* morphotypes we next compared gastrulation and forebrain phenotypes in embryos obtained from reciprocal crosses between cavefish/surface fish males/females. We found that maternal factors present in the egg contribute greatly to the evolution of cavefish gastrulation and subsequent forebrain developmental evolution.

Materials and methods

A. mexicanus embryos

Our surface fish colony originates from rivers in Texas, United States, and our cavefish colony derives from the Pachón cave in San Luis Potosi, Mexico. Embryos were obtained by *in vitro* fertilization and/or natural spawnings induced by changes in water temperature (Elipot et al., 2014). Development of *A. mexicanus* at 24°C is similar and synchronous for both morphotypes (Hinaux et al., 2011). For this study morphological aspects were taken as strict criteria to stage the embryos (number of cells, percentage of epiboly and number of somites). *In vitro* fertilizations were performed to generate reciprocal F1 hybrids by fecundating cavefish oocyte with surface fish sperm (HybCF), and surface fish oocyte with cavefish sperm (HybSF).

Whole mount in situ hybridization (ISH)

ISH was carried out as previously described (Pottin et al., 2011). Digoxigenin- and Fluorescein-labeled riboprobes were prepared using PCR products as templates. Genes of interest were searched in an EST (Expressed sequence tag) library accessible in the laboratory. Clones in library (pCMV-SPORT6 vector): *chordin* (ARA0AAA23YC10), *dkk1b* (ARA0AAA18YA07EM1), *eya2* (ARA0AAA19YL19EM1), *floating-head* (ARA0ACA35YA23), *myoD* (ARA0AAA95YG16), *msgn1* (ARA0ACA49YF15), *no-tail* (ARA0ABA99YL22), *npy* (FO263072), and *vsx1* (ARA0AHA13YJ18). Others: *fgf8* (DQ822511), *lhx9* (EF175738), *shh* (AY661431), *dlx3b (*AY661432), *hcrt (XM_007287820.3)*, *lhx7* (XM_022678613) cDNAs were previously cloned. Cloned for this study: total RNA from *Astyanax* embryos of various stages (2-24 hpf) was reverse-transcribed using the iScript cDNA synthesis kit (Bio-Rad) and amplified using the following primers:

brachyury, FP: CACCGGTGGAAGTACGTGAA, RP: GGAGCCGTCGTATGGAGAAG;

frzb: FP: CTCGTCTGTTCACACGGACA, RP: CACGCTTTAGAATCCGCTGC;

noggin1: FP: CTCGCTACATCATCGCGGTC, RP: ACGAGCACTTGCACTCTGTG;

lefty1: FP: ACCATGGCCTCGTGCCTC; RP: TCAGACCACCGAAATGTTGTCCAC

Full length cDNAs were cloned into the pCS2+ expression vector using the indicated restriction sites:

dkk1b (sites EcoRI and XhoI), FP: GGTGGTGAATTCACCATGTGGCCGGCGGCGCTCTCAGCCCTGACCTTC, RP: ACCACCCTCGAGTCAGTGTCTCTGGCAGGTATGG;

vsx1 (sites XhoI and XbaI), FP: GGTGGTCTCGAGACCATGGAGAAGACACGCGCG, RP: ACCACCTCTAGATCAGTTCTCGTTCTCTGAATCGC;

oep (*tdgf1*) (sites BamHI and XbaI), FP: GGTGGTGGATCCACCATGAGGAGCTCAGTGTTCAGG, RP: ACCACCTCTAGATCAAAGCAGAAATGAAAGGAGGAG.

mRNA injections

In vitro transcription was carried out from PCR products using the SP6 RNA polymerase (mMESSAGE mMACHINE) to generate full length capped mRNA. Dilutions of the mRNA to 150-200ng/µL were prepared in phenol red 0.05%. Embryos at the one cell stage were injected with 5–10 nL of working solutions using borosilicate glass pipettes (GC100F15, Harvard Apparatus LTD) pulled in a Narishige PN-30 Puller (Japan).

Image acquisition and analyses

Whole mount embryos stained by colorimetric and fluorescent ISH were imaged on a Nikon AZ100 multizoom macroscope coupled to a Nikon digital sight DS-Ri1 camera, using the NIS software. Mounted specimens were image on a Nikon Eclipse E800 microscope equipped with a Nikon DXM 1200 camera running under Nikon ACT-1 software. Confocal images were captured on a Leica SP8 microscope with the Leica Application Suite software. Morphometric analyses and cell counting were performed on the Fiji software (Image J). To measure the approximate extent of migration in the vegetal to animal axis (Height) we measured the distance from the margin to the leading cell normalized by the distance from the margin to the animal end (a representation using the expression of *lefty1* at 70% epiboly is shown in **Supplemental figure 1A)**. To estimate the extent of dorsal convergence we measured either the width of the expression domain (for example for *flh*) or the width of gap without expression (for example for *myoD*) normalized by the total width of the embryo (a representation using the expression of *myoD* at 70% epiboly is shown in **Supplemental figure 1B)**. All measurements were normalized, unless otherwise indicated. Another means we used to calculate the width of expression was by measuring the angle (α) of the expression pattern from an animal view, using the center of the opposite site to the expression domain to set the vertex (a

representation using the expression of *chordin* at 50% epiboly is shown in **Supplemental figure 1C)**. Statistical analyses were done in Graph pad prism 5.

qPCR

Total RNA was extracted from 2 hpf cavefish or surface fish embryos with TRIzol reagent (Invitrogen) followed by purification and DNase treatment with the Macherey Nagel NucleoSpinV R RNAII kit. RNA amounts were determined by the Nanodrop 2000c spectrophotometer (Thermo Scientific). 1 µg of total RNA was reverse transcribed in a 20 µL final reaction volume using the High Capacity cDNA Reverse Transcription Kit (Life Technologies) with RNase inhibitor and random primers following the manufacturer's instructions. Quantitative PCR was performed on a QuantStudioTM 12K Flex Real-Time PCR System with a SYBR green detection protocol at the qPCR platform of the Gif CNRS campus. 3 µg of cDNA were mixed with Fast SYBRV R Green Master Mix and 500 nM of each primer in a final volume of 10 µL. The reaction mixture was submitted to 40 cycles of PCR (95°C/20 sec; [95°C/1 sec; 60°C/20 sec] X40) followed by a fusion cycle to analyze the melting curve of the PCR products. Negative controls without the reverse transcriptase were introduced to verify the absence of genomic DNA contaminants. Primers were designed using the Primer-Blast tool from NCBI and the Primer Express 3.0 software (Life Technologies). Primers were defined either in one exon and one exon–exon junction or in two exons span by a large intron. Specificity and the absence of multilocus matching at the primer site were verified by BLAST analysis. The amplification efficiencies of primers were generated using the slopes of standard curves obtained by a fourfold dilution series. Amplification specificity for each real-time PCR reaction was confirmed by analysis of the dissociation curves. Determined Ct values were then exploited for further analysis, with the *Gapdh* gene as reference. Each sample measurement was made in triplicate.

Results

Molecular identity of the gastrula margin in A. mexicanus.

In the zebrafish the embryonic organizer/shield becomes apparent at the prospective dorsal margin of the blastopore right after the epiboly has covered half of the yolk cell (50% epiboly), a stage that coincides with the initiation of the internalization of mesendodermal precursors. In *A. mexicanus* the embryonic shield is not always as morphologically evident as it is for the zebrafish. We studied the expression of genes involved in the establishment of the organizer in the two *A. mexicanus* morphotypes at the equivalent stage by ISH, in order to search for early differences.

First, at 50% epiboly, the inhibitor of the WNT signaling pathway, *Dkk1b*, was expressed in a strikingly different pattern in the two morphs. In the surface fish, *dkk1b* expression was observed at the dorsal margin in two groups of cells separated by a gap in the center (**Figure 1A**), a pattern observed in the majority of the embryos (around 70%; **Figure 1C** blue). In the cavefish, a single central spot of variable extension (**Figure 1B**) was observed in most of the samples analyzed (around 70%; **Figure 1C** red). A minority of embryos of each morphotype showed an intermediate pattern corresponding to a line of positive cells without a clear interruption (not shown, **Figure 1C** green). To interpret this *dkk1b* pattern difference between the two morphs, fluorescent ISH and confocal imaging was performed. In cavefish at 50% epiboly, the *dkk1b*+ cells were already internalized under the dorsal aspect of the margin (**Figure 1D-D'' and 1E, E'**), revealing a precocious internalization process as compared to surface fish.

Chordin is a dorsalizing factor, inhibitor of the BMP pathway. In *A. mexicanus* it is expressed broadly in the dorsal side (**Figure 1F, G**), probably further of the ventral margins of the organizer than it is described in zebrafish (Langdon & Mullins, 2011; Miller-Bertoglio et al., 1997). In surface fish embryos *chordin* expression extended more ventrally than in cavefish (**Figure 1F-H**), as quantified by measuring the angle of expression in an animal view (**Supplemental Figure 1C**). From a dorsal view *chordin* showed a slightly larger extension in the vegetal to animal axis, although not significant (not shown). This *chordin* pattern difference might suggest that convergence towards the dorsal pole is more advanced in cavefish.

Lefty1 is part of a feedback loop regulating nodal signaling activity, involved in axial mesoderm formation and lateral asymmetry establishment (Bisgrove et al., 1999; Meno et al., 1998). In *A. mexicanus* embryos *lefty1* expression was observed in the dorsal margin at 50% epiboly (**Figure 1I, J**). The ventral extension of

lefty1 expression was similarly variable in both morphotypes at this stage (not shown) and no significant differences were observed in the vegetal-animal extension (Height, **Figure 1K**).

We also compared the expression of 3 genes involved in the development of notochord: *floating head* (*flh*), *no-tail* (*ntl*) and *brachyury* (*bra*) (Glickman et al., 2003; Schulte-Merker et al., 1994; Talbot et al., 1995). At 50% epiboly the homeobox gene *flh* showed localized expression in the dorsal margin (**Figure 1L, M**), without differences neither in width nor in height when compared between morphotypes (**Figure 1N**). At the same stage *ntl* and *bra* expression extended homogenously all around the margin (blastopore), hindering the identification of the prospective dorsal side (**Figure 1O, P** and **1Q, R**, respectively). No differences were observed between surface fish and cavefish.

Together these results suggested that internalizing mesodermal lineages were more advanced in CF compared to SF, relative to the percentage of epiboly. To test this hypothesis, we next analyzed the expression of axial mesodermal markers during subsequent stages of gastrulation.

Mesoderm internalization timing in A. mexicanus morphotypes

The EVL (enveloping layer) and YSL (yolk syncytial layer) drive epiboly movements that engulf the yolk cell. Axial mesoderm precursors are mobilized from the dorsal organizer towards the rostral extreme of the embryo (animal pole), migrating in between the YSL and the epiblast (prospective neurectoderm). Since these events are important for the induction and patterning of the neural tube, we compared in detail the process of internalization in *A. mexicanus* morphotypes using markers of different mesodermal populations, always using the percentage of epiboly as reference to stage embryos.

The different patterns observed for *dkk1b* at 50% epiboly in the two morphs were also clear towards mid-gastrulation. In surface fish, the two clusters observed at 50% epiboly began to coalesce at the midline at 70% epiboly (**Figure 2A**), whereas in the cavefish, at the same stage, *dkk1b* expressing cells became more grouped dorsally (**Figure 2B**) and leading cells were more advanced towards the animal pole (**Figure 2C**). At 80% epiboly, *dkk1b*+ cells in the cavefish were close to their final position in the anterior prechordal plate at the rostral end of the embryonic axis (**Figure 2E**). On the other hand, cells expressing *dkk1b* in the surface fish at 80% epiboly (**Figure 2D**) had reached a similar distance than they did in cavefish at 70% epiboly (compare values in **Figure 2F** and **2C**). These expression profiles indicated that even though at 50% epiboly *dkk1b* expression appears very divergent in the two morphotypes, the cellular arrangement observed later on are similar, although always more advanced in the cavefish.

The same analysis was performed at 70% epiboly for the markers *chordin* (**Figure 2G-I**), *lefty1* (**Figure 2J-L**) and *ntl* (**Figure 2M-O**). These 3 genes showed a greater height value of their expression domain in cavefish than in surface fish embryos. This further suggested that at equivalent stages during gastrulation anteroposterior axis formation is more advanced in cavefish.

Next, we wondered if the observed phenotype in the cavefish axial mesoderm also extends to the neighboring paraxial mesoderm, *i.e.*, the mesodermal tissue located laterally. We analyzed the expression of *myoD* and *mesogenin 1* (*msgn1*), two genes coding for bHLH transcription factors required for early specification of myogenic tissue (Weinberg et al., 1996; Yabe and Takada, 2012). In *A. mexicanus*, at mid-gastrulation *myoD* was expressed in two domains, triangular in shape, on both sides of the dorsal axial mesoderm, corresponding to the central gap without expression (**Figure 3A-D**). The height value of the expression domain was higher in cavefish embryos both at 70% and 80% epiboly compared to the surface fish (**Figure 3E**), whereas the central/dorsal gap was larger in the latter at both stages (**Figure 3F**). On the other hand, *msgn1* extended as a ring all around the margin, except on its dorsal aspect, leaving a central gap (**Figure 3G-J**). For *msgn1* no significant differences were found in the height value (**Figure 3K**), but similarly to what was observed for *myoD*, the central gap was reduced in cavefish embryos at 80% epiboly (**Figure 3L**). In order to understand the inter-morph differences observed using these two paraxial mesoderm markers, we performed double ISH. Similar to what was observed in single ISH, *msgn1* expression extended further ventrally than *myoD* (**Figure 3M, O**; compare to insets in **Figures 3A, B, G and H**). Differences also appeared in the vegetal to animal axis, where the larger extension encompassed by *myoD* was clear in both morphs (**Figure 3M, O**). These results suggested that the differences observed in our measurements of paraxial mesoderm extension were mainly due to the cell population expressing *myoD*, but not *msgn1,* which is more advanced towards the animal end of the embryo (**Figure 3N, P)**. In addition, if the size of the central gap where expression of the two paraxial markers is interrupted is taken as a readout of dorsal convergence, these data suggested an earlier convergence and extension in cavefish than in surface fish (at a given stage of epiboly). This could contribute to differences in height values observed with axial mesoderm markers.

A. mexicanus morphotypes exhibit notable differences in axial mesoderm structure

The antero-posterior embryonic axis in *A. mexicanus* is formed after epiboly has been completed, at the bud-stage (10hpf). The prechordal plate and notochord are the anterior and posterior segments of the axial mesoderm, respectively, both important for the induction and patterning of neural fates. To compare

the organization of the axial mesoderm in cave and surface embryos, we analyzed the expression of the markers described in the previous sections, to identify specific segments once the embryonic axis has been formed. Using triple fluorescent *in situ* hybridization, three non-overlapping molecular subdomains were recognized: the anterior prechordal plate or polster labeled by *dkk1b*, the posterior prechordal plate defined by *shh* expression (larger in cavefish as previously described; Pottin et al., 2011; Yamamoto et al., 2004) and the notochord more posteriorly, labeled by *ntl* (**Figure 4A, B**). In addition, *lefty1* expression covered both the anterior and posterior subdomains of the prechordal plate (**Figure 4C-F**). In the posterior prechordal plate *lefty1* and *shh* showed overlapping patterns in both morphotypes (**Figure 4C, D**), whereas *dkk1b* and *lefty1* showed only minimal co-expression anteriorly (**Figure 4E, F**), similarly to what we observed at earlier stages (see **Figure 2 and Supplemental Figure 2**). Moreover, the distribution of polster *dkk1b*-expressing cells was strikingly different between the two morphs. In surface fish they were tightly compacted (**Figure 4A**), while in cavefish they were loosely organized (**Figure 4B**). The number of *dkk1b*-expressing cells, analyzed in confocal sections, were similar in cavefish and surface fish (**Figure 4G**). The distribution of the *dkk1b* cells in the antero-posterior axis, measured by the distance between the first and the last cells (Length A-P), was identical (**Figure 4H**). However, the *dkk1b* positive cells covered a larger extension in the lateral axis (Length lateral) in cavefish embryos (**Figure 4I**), indicating that these cells are arranged at a lower density as compared to surface fish. A similar pattern was observed for the anterior domain of *lefty1* expression (compare **Figures 4C, E** to **4D, F**). Thus, both the anterior/polster (*dkk1b*+) and the posterior part (*shh*+) of the prechordal plate are laterally expanded in cavefish.

Next, other differences in size or position of axial mesoderm segments at bud stage were explored. The distance from the anterior-most polster cell expressing *dkk1b* to the leading notochord cell expressing *ntl* was identical in the two morphs (**Supplemental figure 3 A-C**). Polster cells expressing *dkk1b* laid just beneath the cells of the anterior neural plate border (*dlx3b*+) in both morphotypes (**Supplemental figure 3 D, E**). The extension of the notochord was also measured. At bud stage *ntl* and *bra* expression labeled the notochord in its whole extension (**Figure 4J, K** and not shown). On the other hand, *flh* was expressed in the posterior end and in a small cluster of the rostral notochord (**Figure 4L, M**) (plus two bilateral patches in the neural plate probably corresponding to the prospective pineal gland in the diencephalon). For the three notochordal markers, the distance from the rostral expression boundary to tail bud (normalized by the size of the embryo) was larger in cavefish compared to surface fish (**Figure 4N-P**). In line with our observations of axial and paraxial mesoderm markers during mid-gastrulation (**Figure 2-3**), these results suggest a delayed convergence and extension in the surface fish compared to cavefish.

"Potential" effects of heterochrony in gastrulation and gene expression dynamics on brain development

In zebrafish embryos *dkk1b* expression in the prechordal plate becomes downregulated from early somitogenesis (Hashimoto et al., 2000). Our observations of heterochronic gastrulation events prompted us to search for potential differences also in the disappearance of *dkk1b* expression later on. In surface fish *dkk1b* was still expressed in all embryos at the 6 and 8 somite stage (13/13, **Figure 5A** and 11/11, **Figure 5C,** respectively). In contrast, in cavefish *dkk1b* expression was observed only in 46% of the embryos at 6 somites (6/13, always with low signal level) (**Figure 5B**) and it was absent in the majority of embryos at 8 somite stage, with only 19% of weakly positive embryos (4/21, not shown) (**Figure 5D**).

Given the major spatio-temporal differences in *dkk1b* expression pattern observed from the onset of gastrulation to the end of neurulation between cave and surface embryos, we also examined its expression levels through qPCR experiments. While at 50% epiboly *dkk1b* transcript levels were similar in the two morphs (0.95 fold, NS), at bud stage *dkk1b* levels were almost four times lower in cavefish than in surface fish embryos (0.27 fold).

Since *dkk1b* is a strong inhibitor of WNT signaling, with conserved functions in the regulation of brain development (Hashimoto et al., 2000; Lewis et al., 2008), these differences both in expression levels and timing of downregulation may have downstream consequences in forebrain morphogenesis. Previous data from our laboratory have described a heterochronic onset of *fgf8* expression at the anterior neural border (Pottin et al., 2011). At 4 somite stage (when *fgf8* can be detected in cavefish, but not in surface fish embryos) we observed that *dkk1b* expressing cells abut on and seem to restrict antero-ventrally the cells expressing *fgf8* (**Figure 5E, E'**), suggesting a possible interaction between the WNT and FGF signaling pathways at this level.

Maternal control of early development

The earliest developmental events including the first cell divisions, breaking of symmetries (except lateralization) and induction of the embryonic organizer rely exclusively on maternal factors present in the oocyte long before fertilization. The findings above showing early convergence, extension and internalization of mesodermal cell populations in the cave morphs, and differences in the spatio-temporal gene regulation in tissues derived from the organizer prompted the examination of precocious

embryogenesis and the investigation of maternal components. The inter-fertility between *A. mexicanus* morphotypes offers a powerful system to study the potential contribution of these maternally-produced factors to phenotypic evolution (Ma et al., 2018). We compared gastrulation progression in F1 hybrid embryos obtained from fertilization of surface fish eggs with cavefish sperm (HybSF), and cavefish eggs with surface fish sperm (HybCF). In principle, phenotypic correspondence to the maternal morphotype indicates a strong maternal effect. Results obtained in F1 hybrids were compared to those obtained from wild type morphs in previous sections.

First, the expression patterns of *dkk1b* were compared. At 50% epiboly the percentages of the phenotypic categories (described in **Figure 1**) in hybrid embryos were strikingly similar to those of their maternal morphotypes (**Figure 6C**), with the majority of HybSF presenting two spots of *dkk1b* expression (**Figure 6A**) as surface fish embryos (**Figure 1A**), whereas most of HybCF embryos showed only one continuous expression domain (**Figure 6B**). At 70% epiboly the results followed the same trend. In HybSF embryos the two domains of *dkk1b* expressing cells start to join dorsally, with little advancement towards the animal pole (**Figure 6D**), similar to surface embryos (**Figure 2A**). In contrast, HybCF were more alike cavefish embryos (**Figure 2B**), with cells grouped dorsally close to the animal end (**Figure 6E**). Analyses of the distance reached by the leading cell showed significant differences between the two reciprocal hybrids types, which were identical to their maternal morphs (**Figure 6F**). The expression of *lefty1* and *ntl* at 70% epiboly was also compared in F1 hybrids (**Figure 6G-I** and **6J-L**, respectively). The advancement of axial mesoderm populations labeled by the two markers was significantly increased in HybCF compared to HybSF, with height values akin to their respective maternal morphs (**Figure 6I, L**). These results indicate that spatio-temporal differences observed during gastrulation between cavefish and surface fish fully depend on maternal contribution.

Finally, we sought to test whether forebrain phenotypes described previously in cavefish at later developmental stages could be also influenced by maternal effects, as a long-lasting consequence of the maternal influence during gastrulation. Hypothalamic, eye and olfactory epithelium development were analyzed in reciprocal hybrids between 15hpf and 24hpf.

Inter-morph variations in the expression domains of the LIM-homeodomain transcription factors *Lhx9* and *Lhx7* drive changes in Hypocretin and NPY neuropeptidergic neuronal patterning in the hypothalamus, respectively (Alié et al., 2018). We therefore compared expression domains of *Lhx9* (size of the hypothalamic domain at 15 hpf; brackets in **Figure 7A, B**) and *Lhx7* (number of positive cells at 24 hpf in the hypothalamic acroterminal domain; dotted circles in **Figure 7D, E**) and the numbers of their respective

neuropeptidergic Hypocretin and NPY derivatives in the reciprocal hybrids and their parental morphotypes. In all four cases the analyses showed strong significant differences between cavefish and surface fish, as previously described (Alié et al., 2018) (**Figure 7A to 7L**, *** for each). In order to help the visualization and interpretation of the F1 hybrid data, simplified plots were generated (**Figure 7C'F'I' and L'**) with the mean values for cavefish and surface fish in the extremes (red and blue dots, respectively), an average black dot representing the expected value for the phenotype if there is no effect of any kind (maternal, paternal or allelic dominance), and the HybSF and HybCF values (light blue and pink respectively). If experimental values are closer to the maternal morphotype, it can be interpreted as the phenotype being under maternal regulation. Other possibilities, such as a mix of maternal and zygotic influence, or recessive or dominant effects in heterozygotes can also be interpreted.

For *Lhx9* and *Lhx7,* hybrids values were similar and intermediate between the cave and surface morphs (**Figure 7C, F**), with a slight deviation towards the surface morph, more evident for the HybSF (**Figure C' and F'**). For Hypocretin and NPY neuropeptidergic lineages derived from *Lhx9* and *Lhx7*-expressing progenitors, a significant difference in neuron numbers existed between reciprocal hybrids (**Figure 7GHI and JKL**, respectively, ***** for each), suggesting the involvement of maternal components. Moreover, the number of Hypocretin neurons in HybSF and the number of NPY neurons in HybCF were identical to their maternal morphotype, respectively, whereas values for their reciprocal hybrids were close to the theoretical intermediate value (**Figure 7I'L'**). These results suggest that maternal determinants impact at least in part hypothalamic neuronal differentiation, possibly together with other, complex, allelic dominance or zygotic mechanisms.

In cavefish, the smaller size of the eye primordium and the larger olfactory epithelia compared to surface fish are also due to modifications of signals emanating from midline organizers, including shh and fgf8 (Hinaux et al., 2016; Pottin et al., 2011; Yamamoto et al. , 2004). The size of these sensory structures were measured in reciprocal hybrids to test if the cascade of events affected by the maternal determinants also has an impact later in development. First, in F1 hybrids, the size of the eye ball and the size of the lens at 24 hpf (dotted lines in **Figure 7M, N;** DAPI stained embryos) were intermediate between those from the parental morphs (**Figure 7O, P**), without significant differences between the hybrids in the ANOVA test. Of note, when considering only the hybrids, the Mann Whitney test showed a significant difference in lens size (**Figure 7P**, golden star p= 0.0202), suggesting a reminiscence of maternal effect. In the plots of mean distribution for Eye ball size the hybrid values were located close to the expected mean (**Figure 7O'**). In the plot for lens size however, the hybrid values were slightly deviated towards the cavefish mean (**Figure**

7P'), suggesting also a dominance of cavefish alleles involved in lens development. Finally, the size of the olfactory epithelium at 24 hpf was similar in HybSF and HybCF (**Figure 7Q to S';** DAPI staining) and (**Figure 7T to V';** ISH to *eya2*). In both types of read-outs, the mean values for hybrids appeared shifted towards surface fish values (**Figure S', V'**), suggesting a dominance of the surface fish alleles involved in olfactory epithelium development.

Taken together, these results indicate that the effect of maternal determinants are fully penetrant at least to final stages of gastrulation, suggesting that mRNAs and proteins present in the oocyte must vary between the two *Astyanax* morphotypes. At later developmental stages the maternal effect appears to be "diluted" by other mechanisms regulating gene expression and morphogenesis, although some differences can still be observed.

Towards identification of varying maternal factors in cavefish

A candidate approach was undertaken on a restricted number of genes to identify differentially-expressed maternal factors in the two *Astyanax* morphs by qPCR, on 2hpf embryos. Since nuclear localization of maternal beta-catenin in the future dorsal side is the first indication of dorso-ventral polarity in the embryo (Bellipanni, et al., 2006), the two *β-catenin* genes, *ctnnb1* and *ctnnb2* were analyzed. We also included *Oep* (*one-eyed pinhead,* also named *tdgf1*), a Nodal co-receptor necessary for *dkk1b* induction and shield formation and whose maternal and zygotic mutant (*MZoep*) shows defects in margin internalization and fate specification in zebrafish (Carmany-Rampey & Schier, 2001; Zhang et al., 1998); as well as the maternal ventralizing transcription factor *Vsx1* (*Visual System homeobox 1*) which regulates *flh* and *ntl* expression and is involved in axial *versus* paraxial mesoderm specification and migration (He et al., 2014; Xu, He et al, 2014).

Ctnnb1 and *ctnnb2* transcripts levels were similar in cavefish and surface fish embryos (0.70 and 0.73 fold in cavefish, NS), while both *Vsx1* and *Oep* mRNA levels were significantly reduced in cavefish (0.40 and 0.57 fold in cavefish, respectively). This demonstrates that expression differences exist for maternally-expressed factors between cave and surface embryos just after fertilization, and before the mid-blastula transition. To test for a possible role of these two maternal down-regulated transcripts in the cavefish gastrulation phenotype, we performed overexpression experiments through mRNA injection at one cell stage in cavefish eggs. As read-out of these rescue experiments, *dkk1b* expression was examined at 50% and 70% epiboly. *Vsx1*-injected and *Oep*-injected embryos were similar to control cavefish embryos in

terms of spatio-temporal *dkk1b* pattern, although some signs of disorganization were visible on several specimens (not shown). Thus, a role for *Vsx1* and *Oep* maternal transcripts in the variations of *dkk1b* expression observed between the two *Astyanax* morphs is unlikely. These preliminary data pave the way for future larger scale transcriptomic analyses.

Discussion

Astyanax mexicanus has become an excellent model to uncover developmental mechanisms leading to phenotypic evolution. Modifications in midline signaling centers during early embryogenesis have led to troglomorphic adaptations in cavefish, including eye degeneration, larger olfactory epithelia and increased number of taste buds. In addition to previously described modifications in the expression of the signaling molecules *shh*, *fgf8*, and *bmp4*, here we show striking temporal, spatial and quantitative differences in the expression of *dkk1b*, an inhibitor of the WNT signaling pathway and we explore the idea that maternally-regulated gastrulation might be a source of variation contributing to cavefish morphological evolution.

Prechordal plate and forebrain patterning

Genetic manipulations, tissue ablation and transplantation experiments have demonstrated the importance of the prechordal plate as a signaling center involved in the patterning of the basal forebrain (Heisenberg & Nüsslein-Volhard, 1997; Pera & Kessel, 1997). In fish, the prechordal plate is organized in two domains: the rostral polster (Kimmel et al., 1995) and a posterior domain abutting caudally with the notochord. In *A. mexicanus* the expression of *shh* in the posterior prechordal plate occupies a wider domain in the cavefish compared to surface fish (Pottin et al., 2011; Yamamoto 2004), and enhanced shh signaling has pleiotropic effects in in the development of head structures in the cavefish (Yamamoto et al., 2009). Here we showed that the anterior domain of the prechordal plate is a source of the morphogen dkk1b, whose expression is complementary to that of *shh* (and *fgf8*) at the neural plate stage. At this stage, *dkk1b* expressing cells are organized as a compact cluster in the surface fish, while in the cavefish they are more loosely distributed, and with lower levels of *dkk1b* transcripts. Inhibition of WNT signaling in the anterior brain is critical for patterning and morphogenesis. Mouse or *Xenopus* embryos with impaired Dkk1 function lack anterior brain structures (Glinka et al., 1998; Mukhopadhyay et al., 2001), whereas misexpression of *dkk1b* in zebrafish embryos produce anteriorization of the neurectoderm, including enlargement of eyes (Shinya et al., 2000). Head development is sensitive to WNT signaling dosage (Lewis et al., 2008), and the temporal variations of *dkk1b* expression we observed here might contribute to forebrain evolution in cavefish. Indeed, the timing and intensity of WNT (this work) and BMP (Hinaux et al., 2016) signaling at the anterior pole of the axial mesoderm must instruct the fate and morphogenetic

movements of overlying anterior neural plate progenitors destined to form the optic region and the hypothalamus, as well as the placode derivatives (Bielen et al., 2017; Rétaux et al., 2013).

Embryonic axis formation

The establishment of the embryonic axes and primordial germ layers occurs through complex morphogenetic cell rearrangements during gastrulation (Schier and Talbot, 2005; Solnica-Krezel and Sepich, 2012). The main outcomes of gastrulation are the spreading of the blastodermal cells, internalization of endomesoderm precursors and the elongation of the antero-posterior embryonic axis. We hypothesized that the differences observed in the axial mesoderm of *A. mexicanus* morphotypes may be the consequence of upstream events during gastrulation. We systematically compared the process of gastrulation by analyzing the expression of markers of different mesodermal population along its course. At equivalent stages, as judged by the percentage of epiboly, we observed that the advancement of internalized tissues migrating in the vegetal to animal direction is more precociously in cavefish embryos than in surface fish. Interestingly, this finding was not only restricted to axial mesodermal elements, but also applied to laterally adjacent paraxial mesoderm, suggesting a global phenomenon. From the different measurements performed, we concluded that dorsal convergence, earlier internalization and anteroposterior extension might be the driving forces leading to the more advanced phenotype observed in cavefish gastrulas. Interestingly, the differences in hypoblast movements we observed, relative to the percentage of epiboly covering, highlight the uncoupling between gastrulation cells movements and the epiboly itself, as spectacularly illustrated in the extreme example of annual killifish embryogenesis (Pereiro et al., 2017). We suggest that these temporal variations in gastrulation events might later correlate to differences observed in the off-set of *dkk1b* expression, occurring in cavefish before the 6 somite stage and in surface fish after the 8 somite stage. This possibly is also associated to the previously described heterochrony on *fgf8* expression in the anterior neural border, two hours earlier in the cavefish (Pottin et al., 2011) and which has an impact on eye morphogenesis.

Cellular interactions during gastrulation

Gastrulation involves dynamic interactions between different cell populations, while as they move, cells are exposed to changing signals in their immediate environment. Individual interactions between tissues, such as the migration of the hypoblast using epiblast as substrate (Smutny et al., 2017) and the influences

that the blastodermal cells receive from direct physical contact with the extraembryonic EVL (Reig et al., 2017) and YSL (Carvalho & Heisenberg, 2010) must be integrated as gastrulation proceeds. In addition, the prechordal plate has been described as a cell population undergoing collective migration, implying numerous cell-cell interactions between prechordal cells themselves (Dumortier et al., 2012; T. Zhang et al., 2014). Genetic dissection of the parameters regulating prechordal plate migration (coherence, motility and directionality) (Kai et al., 2008), as well as the identification of intrinsic properties of the moving group (Dumortier et al., 2012), have helped understanding the molecular and cellular aspects regulating their migration. The markers we used here to label the prechordal plate during gastrulation suggest that within this domain *lefty1*-expressing cells follow collective migration as a cohesive group, whereas *dkk1b*+ cells constitute a more dispersed group, especially in the cavefish, and as also recently observed by Ren et al., 2018. Moreover, increased Nodal signaling and changed cell distribution have been reported in the organizer in cavefish embryos (Ren et al., 2018). Together with our observation of the apparently early internalization of axial mesoderm cells in cavefish, collectively these data suggest that the structural variations observed in the cavefish prechordal plate may relate to differential physical and adhesion properties of the organizer/prechordal cells in the two morphs. Live imaging will be necessary to better compare the properties of prechordal plate cells in cavefish and surface fish. Moreover, detailed analyses of expression of molecules involved in cell adhesion, such as snails and cadherins (Blanco et al., 2007; Montero et al., 2005; Shimizu et al., 2005), as well as those involved in membrane protrusion formation, such as β-actin (Giger & David, 2017), will help to explore the possibility that divergence in the intrinsic properties of prechordal plate cells may account for cavefish phenotypic evolution.

Maternal control of gastrulation

Regardless of the striking morphological evolution observed in *A. mexicanus* morphotypes, their time of divergence has been estimated to be recent (less than 20.000 years ago) (Fumey et al., 2018). The inter-fertility, reminiscent of such a short time of divergence between the two morphs, has allowed the use of hybrids for the identification of the genetic basis behind phenotypic change (Casane & Rétaux, 2016; Protas et al., 2006).

Since early embryonic development is driven by maternal determinants present in the oocyte previous to fecundation, the cross fertility in *A. mexicanus* species is a valuable tool to obtain information about the contribution of maternal effect genes to phenotypic evolution (Ma et al., 2018). Our analyses in F1 reciprocal hybrids demonstrated that the developmental evolution of gastrulation in cavefish is dependent

on maternal factors. This encouraged us to search for genes differentially expressed in embryos at two hours post-fertilization, before zygotic genes become transcriptionally active. In qPCR analyses the candidate genes beta-catenin 1 and 2, involved in the establishment of the organizer (Kelly et al., 2000), did not show significantly different levels of expression. Two other genes, *oep* and *vsx1*, implicated in the development of the prechordal plate (Gritsman et al., 1999; Xu et al., 2014) showed reduced levels in cavefish compared to surface fish. However, overexpression of these two candidate genes by mRNA injection in cavefish was not able to recapitulate the gastrulation phenotype observed in the surface fish. Ma et al. (2018) have also recently described increased *pou2f1b*, *runx2b*, and *axin1* mRNA levels in unfertilized cavefish eggs as compared to surface fish eggs. Although these results clearly confirm predictions about differentially expressed maternal genes, more systematic comparative transcriptomic analyses are now necessary to identify maternal signaling factors and pathways that impact cavefish developmental evolution. In addition, modified gene expression could be due to differential *cis*-regulation of gene expression, which for maternal effect genes in evolutionary context has not been explored yet to our knowledge in any species.

Our results on the impact of maternal determinants in forebrain morphogenesis are puzzling. Regarding the eye phenotype, our results are consistent with those of Ma et al., 2018 who examined maternal genetic effects in cavefish eye development and degeneration: at embryonic stages (12-24hpf), eye size and shape do not seem to be influenced by maternal factors. However, later larval lens apoptosis and eye regression appear to be under maternal control (Ma et al., 2018). This fits with our finding that lens size at 24hpf differs between reciprocal F1 hybrids. Indeed, the defective and apoptotic lens in cavefish is the trigger for eye degeneration (Yamamoto & Jeffery, 2000) and midline shh signaling indirectly impacts this lens-directed process (Hinaux et al., 2016; Ren et al., 2018; Yamamoto et al., 2004). Hence, the lens phenotype, but not the retina (which is in fact relatively properly formed and healthy in cavefish embryos), probably results from maternally-controlled developmental evolution in cavefish. This renders even more mysterious the long-standing question of what regulates the lens defects and apoptotic process in cavefish embryos.

More generally, regarding hypothalamic, eye and olfactory development that we have analyzed, our interpretation is that although maternal factors greatly influence early developmental decisions, later phenotypes become “diluted” due to other mechanisms entering into play. We suggest that once zygotic genome takes control over development, allelic dominance has a major impact on the phenotypes we observed from 15 hpf onwards, although we could still observe some tendency to maternally-controlled

phenotype in hybrids for some of the traits analyzed. Of note in *Astyanax,* some behavioral traits in adults have already been shown to be under parental inheritance (Yoshizawa et al., 2012): the vibration attraction behavior and its underlying sensory receptors (the neuromasts) are under paternal inheritance in cavefish originating from the Pachón cave, while they are under maternal inheritance in cavefish originating from the Los Sabinos cave. These examples underscore the different levels of developmental regulation that must interact to produce a hybrid phenotype.

The study of the impact of maternal components in the morphological and developmental evolution of species is open. To our knowledge, besides *Astyanax* cavefish, only one study reported a maternal contribution regulating the developmental trajectory of entry into diapause in a killifish (Romney & Podrabsky, 2017). Thus *Astyanax* cavefish appear as a proper model to disentangle the very early genetic and embryonic mechanisms of morphological evolution.

Acknowledgements

We thank Stéphane Père, Victor Simon and Krystel Saroul for care of our *Astyanax* colony, and all the members of the DECA team for fruitful discussions and important suggestions to our study. This work has benefited from the facilities and expertise of the QPCR platform of I2BC, Gif sur Yvette. Grant support: FRM (Equipe FRM DEQ20150331745 RETAUX) and CNRS.

References

Alié, A., Devos, L., Torres-Paz, J., Prunier, L., Boulet, F., Blin, M., … Retaux, S. (2018). Developmental evolution of the forebrain in cavefish, from natural variations in neuropeptides to behavior. *eLife*, *7*. http://doi.org/10.7554/eLife.32808

Bellipanni, G. Varga, M., Maegawa, S., Imai, Y., Kelly, C., Myers, AP., Chu, F., Talbot, W. and Weinberg, E. (2006). Essential and opposing roles of zebrafish β-catenins in the formation of dorsal axial structures and neurectoderm. *Development*, *133*(7), 1299–1309. http://doi.org/10.1242/dev.02295

Bielen, H., Pal, S., Tole, S., & Houart, C. (2017). Temporal variations in early developmental decisions: an engine of forebrain evolution. *Current Opinion in Neurobiology*, *42*, 152–159. http://doi.org/10.1016/J.CONB.2016.12.008

Bisgrove, B. W., Essner, J. J., & Yost, J. H. (1999). Regulation of midline development by antagonism of lefty and nodal signaling. *Development*, *126*(14), 3253–3262.

Blanco, M. J., Barrallo-Gimeno, A., Acloque, H., Reyes, A. E., Tada, M., Allende, M. L., … Nieto, M. A. (2007). Snail1a and Snail1b cooperate in the anterior migration of the axial mesendoderm in the zebrafish embryo. *Development (Cambridge, England)*, *134*(22), 4073–81. http://doi.org/10.1242/dev.006858

Blin, M., Tine, E., Meister, L., Elipot, Y., Bibliowicz, J., Espinasa, L., & Rétaux, S. (2018). Developmental evolution and developmental plasticity of the olfactory epithelium and olfactory skills in Mexican cavefish. *Developmental Biology*. http://doi.org/10.1016/J.YDBIO.2018.04.019

Carmany-Rampey, A., & Schier, A. F. (2001). Single-cell internalization during zebrafish gastrulation. *Current Biology*, *11*(16), 1261–1265. http://doi.org/10.1016/S0960-9822(01)00353-0

Carvalho, L., & Heisenberg, C. P. (2010). The yolk syncytial layer in early zebrafish development. *Trends in Cell Biology*, *20*(10), 586–592. http://doi.org/10.1016/j.tcb.2010.06.009

Casane, D., & Rétaux, S. (2016). Evolutionary Genetics of the Cavefish Astyanax mexicanus. *Advances in Genetics*, *95*, 117–159. http://doi.org/10.1016/BS.ADGEN.2016.03.001

Dumortier, J. G., Martin, S., Meyer, D., Rosa, F. M., & David, N. B. (2012). Collective mesendoderm migration relies on an intrinsic directionality signal transmitted through cell contacts. *Proceedings*

of the National Academy of Sciences, *109*(42), 16945–16950. http://doi.org/10.1073/pnas.1205870109

Elipot, Y., Hinaux, H., Callebert, J., Launay, J.-M., Blin, M., & Rétaux, S. (2014). A mutation in the enzyme monoamine oxidase explains part of the Astyanax cavefish behavioural syndrome. *Nature Communications*, *5*(1), 3647. http://doi.org/10.1038/ncomms4647

Elipot, Y., Legendre, L., Père, S., Sohm, F., & Rétaux, S. (2014). *Astyanax* Transgenesis and Husbandry: How Cavefish Enters the Laboratory. *Zebrafish*, *11*(4), 291–299. http://doi.org/10.1089/zeb.2014.1005

Elliott, W. R. (2018). The Astyanax caves of Mexico. Cavefishes of Tamaulipas, San Luis Potosi, and Guerrero. Association for Mexican cave studies Bulletin 26.

Fumey, J., Hinaux, H., Noirot, C., Thermes, C., Rétaux, S., & Casane, D. (2018). Evidence for late Pleistocene origin of Astyanax mexicanus cavefish. *BMC Evolutionary Biology*, *18*(1), 43. http://doi.org/10.1186/s12862-018-1156-7

García-Calero, E., Fernández-Garre, P., Martínez, S., & Puelles, L. (2008). Early mammillary pouch specification in the course of prechordal ventralization of the forebrain tegmentum. *Developmental Biology*, *320*(2), 366–377. http://doi.org/10.1016/j.ydbio.2008.05.545

Giger, F. A., & David, N. B. (2017). Endodermal germ-layer formation through active actin-driven migration triggered by N-cadherin. *Proceedings of the National Academy of Sciences*, *114*(38), 201708116. http://doi.org/10.1073/pnas.1708116114

Glickman, N. S., Kimmel, C. B., Jones, M., & Adams, R. J. (2003). Shaping the zebrafish notochord. *Development*, *130*(5), 873–887. http://doi.org/10.1242/dev.00314

Glinka, A., Wu, W., Delius, H., Monaghan, A. P., Blumenstock, C., & Niehrs, C. (1998). Dickkopf-1 is a member of a new family of secreted proteins and functions in head induction. *Nature*, *391*(6665), 357–362. http://doi.org/10.1038/34848

Gritsman, K., Zhang, J., Cheng, S., Heckscher, E., Talbot, W. S., & Schier, A. F. (1999). The EGF-CFC protein one-eyed pinhead is essential for nodal signaling. *Cell*, *97*(1), 121–132. http://doi.org/10.1016/S0092-8674(00)80720-5

Hashimoto, H., Itoh, M., Yamanaka, Y., Yamashita, S., Shimizu, T., Solnica-Krezel, L., … Hirano, T. (2000).

Zebrafish Dkk1 functions in forebrain specification and axial mesendoderm formation. *Developmental Biology*, *217*(1), 138–152. http://doi.org/10.1006/dbio.1999.9537

He, Y., Xu, X., Zhao, S., Ma, S., Sun, L., Liu, Z., & Luo, C. (2014). Maternal control of axial-paraxial mesoderm patterning via direct transcriptional repression in zebrafish. *Developmental Biology*, *386*(1), 96–110. http://doi.org/10.1016/j.ydbio.2013.11.022

Heisenberg, C. P., & Nüsslein-Volhard, C. (1997). The function of silberblick in the positioning of the eye anlage in the zebrafish embryo. *Developmental Biology*, *184*(1), 85–94. http://doi.org/10.1006/dbio.1997.8511

Hinaux, H., Devos, L., Blin, M., Elipot, Y., Bibliowicz, J., Alié, A., & Rétaux, S. (2016). Sensory evolution in blind cavefish is driven by early embryonic events during gastrulation and neurulation. *Development*, *143*(23), 4521–4532. http://doi.org/10.1242/dev.141291

Hinaux, H., Pottin, K., Chalhoub, H., Père, S., Elipot, Y., Legendre, L., & Rétaux, S. (2011). A Developmental Staging Table for *Astyanax mexicanus* Surface Fish and Pachón Cavefish. *Zebrafish*, *8*(4), 155–165. http://doi.org/10.1089/zeb.2011.0713

Jaggard, J. B., Stahl, B. A., Lloyd, E., Prober, D. A., Duboue, E. R., & Keene, A. C. (2018). Hypocretin underlies the evolution of sleep loss in the Mexican cavefish. *eLife*, *7*. http://doi.org/10.7554/eLife.32637

Kai, M., Heisenberg, C.-P., & Tada, M. (2008). Sphingosine-1-phosphate receptors regulate individual cell behaviours underlying the directed migration of prechordal plate progenitor cells during zebrafish gastrulation. *Development*, *135*(18), 3043–3051. http://doi.org/10.1242/dev.020396

Kelly, C., Chin, a J., Leatherman, J. L., Kozlowski, D. J., & Weinberg, E. S. (2000). Maternally controlled (beta)-catenin-mediated signaling is required for organizer formation in the zebrafish. *Development (Cambridge, England)*, *127*, 3899–3911.

Kimmel, C. B., Ballard, W. W., Kimmel, S. R., Ullmann, B., & Schilling, T. F. (1995). Stages of embryonic development of the zebrafish. *Developmental Dynamics : An Official Publication of the American Association of Anatomists*, *203*(3), 253–310. http://doi.org/10.1002/aja.1002030302

Langdon, Y. G., & Mullins, M. C. (2011). Maternal and Zygotic Control of Zebrafish Dorsoventral Axial Patterning. *Annual Review of Genetics*, *45*(1), 357–377. http://doi.org/10.1146/annurev-genet-110410-132517

Lewis, S. L., Khoo, P.-L., De Young, R. A., Steiner, K., Wilcock, C., Mukhopadhyay, M., … Tam, P. P. L. (2008). Dkk1 and Wnt3 interact to control head morphogenesis in the mouse. *Development (Cambridge, England)*, *135*(10), 1791–801. http://doi.org/10.1242/dev.018853

Ma, L., Strickler, A. G., Parkhurst, A., Yoshizawa, M., Shi, J., & Jeffery, W. R. (2018). Maternal genetic effects in Astyanax cavefish development. *Developmental Biology*, *441*(2), 209–220. http://doi.org/10.1016/J.YDBIO.2018.07.014

Meno, C., Shimono, A., Saijoh, Y., Yashiro, K., Mochida, K., Ohishi, S., … Hamada, H. (1998). lefty-1 Is Required for Left-Right Determination as a Regulator of lefty-2 and nodal. *Cell*, *94*(3), 287–297. http://doi.org/10.1016/S0092-8674(00)81472-5

Menuet, A., Alunni, A., Joly, J., Jeffery, W. R., & Rétaux, S. (2007). Expanded expression of Sonic Hedgehog in Astyanax cavefish : multiple consequences on forebrain development and evolution, *855*, 845–855. http://doi.org/10.1242/dev.02780

Miller-Bertoglio, V. E., Fisher, S., Sánchez, A., Mullins, M. C., & Halpern, M. E. (1997). Differential Regulation ofchordinExpression Domains in Mutant Zebrafish. *Developmental Biology*, *192*(2), 537–550. http://doi.org/10.1006/DBIO.1997.8788

Mitchell, R. W., Russell, W. H. and Elliott, W. R. (1977). Mexican eyeless characin fishes, genus Astyanax: environment, distribution, and evolution. Spec. Publ. Mus. Texas Tech. Univ 12, 1-89.

Montero, J.-A. (2005). Shield formation at the onset of zebrafish gastrulation. *Development*, *132*(6), 1187–1198. http://doi.org/10.1242/dev.01667

Mukhopadhyay, M., Shtrom, S., Rodriguez-Esteban, C., Chen, L., Tsukui, T., Gomer, L., … Westphal, H. (2001). *Dickkopf1 Is Required for Embryonic Head Induction and Limb Morphogenesis in the Mouse*. *Developmental Cell* (Vol. 1):423-434.

Nojima, H., Shimizu, T., Kim, C. H., Yabe, T., Bae, Y. K., Muraoka, O., … Hibi, M. (2004). Genetic evidence for involvement of maternally derived Wnt canonical signaling in dorsal determination in zebrafish. *Mechanisms of Development*, *121*(4), 371–386. http://doi.org/10.1016/j.mod.2004.02.003

Pera, E. M., & Kessel, M. (1997). Patterning of the chick forebrain anlage by the prechordal plate. *Development (Cambridge, England)*, *124*(20), 4153–62. Retrieved from http://www.ncbi.nlm.nih.gov/pubmed/9374411

Pereiro, L., Loosli, F., Fernández, J., Härtel, S., Wittbrodt, J., & Concha, M. L. (2017). Gastrulation in an annual killifish: Molecular and cellular events during germ layer formation in Austrolebias. *Developmental Dynamics*, *246*(11), 812–826. http://doi.org/10.1002/dvdy.24496

Pottin, K., Hinaux, H., & Rétaux, S. (2011). Restoring eye size in Astyanax mexicanus blind cavefish embryos through modulation of the Shh and Fgf8 forebrain organising centres, *2476*, 2467–2476. http://doi.org/10.1242/dev.054106

Protas, M. E., Hersey, C., Kochanek, D., Zhou, Y., Wilkens, H., Jeffery, W. R., … Tabin, C. J. (2006). Genetic analysis of cavefish reveals molecular convergence in the evolution of albinism. *Nature Genetics*, *38*(1), 107–111. http://doi.org/10.1038/ng1700

Puelles, L., & Rubenstein, J. L. R. (2015). A new scenario of hypothalamic organization: rationale of new hypotheses introduced in the updated prosomeric model. *Frontiers in Neuroanatomy*, *9*(MARCH). http://doi.org/10.3389/fnana.2015.00027

Reig, G., Cerda, M., Sepúlveda, N., Flores, D., Castañeda, V., Tada, M., … Concha, M. L. (2017). Extra-embryonic tissue spreading directs early embryo morphogenesis in killifish. *Nature Communications*, *8*, 1–14. http://doi.org/10.1038/ncomms15431

Ren, X., Hamilton, N., Müller, F., & Yamamoto, Y. (2018). Cellular rearrangement of the prechordal plate contributes to eye degeneration in the cavefish. *Developmental Biology*, *441*(2), 221–234. http://doi.org/10.1016/J.YDBIO.2018.07.017

Rétaux, S., Bourrat, F., Joly, J.-S., & Hinaux, H. (2013). Perspectives in Evo-Devo of the Vertebrate Brain. In *Advances in Evolutionary Developmental Biology* (pp. 151–172). Hoboken, NJ, USA: John Wiley & Sons, Inc. http://doi.org/10.1002/9781118707449.ch8

Romney, A. L., & Podrabsky, J. E. (2017). Transcriptomic analysis of maternally provisioned cues for phenotypic plasticity in the annual killifish, Austrofundulus limnaeus, *8*. http://doi.org/10.1186/s13227-017-0069-7

Schier, A. F., & Talbot, W. S. (2005). Molecular Genetics of Axis Formation in Zebrafish. *Annual Review of Genetics*, *39*(1), 561–613. http://doi.org/10.1146/annurev.genet.37.110801.143752

Schulte-Merker, S., Hammerschmidt, M., Beuchle, D., Cho, K. W., De Robertis, E. M., & Nüsslein-Volhard, C. (1994). Expression of zebrafish goosecoid and no tail gene products in wild-type and mutant no tail embryos. *Development (Cambridge, England)*, *120*(4), 843–852.

Shimizu, T., Yabe, T., Muraoka, O., Yonemura, S., Aramaki, S., Hatta, K., … Hibi, M. (2005). E-cadherin is required for gastrulation cell movements in zebrafish. *Mechanisms of Development*, *122*(6), 747–63. http://doi.org/10.1016/j.mod.2005.03.008

Shinya, M., Eschbach, C., Clark, M., Lehrach, H., & Furutani-Seiki, M. (2000). Zebrafish Dkk1, induced by the pre-MBT Wnt signaling, is secreted from the prechordal plate and patterns the anterior neural plate. *Mechanisms of Development*, *98*(1–2), 3–17. http://doi.org/10.1016/S0925-4773(00)00433-0

Smutny, M., Ákos, Z., Grigolon, S., Shamipour, S., Ruprecht, V., Čapek, D., … Heisenberg, C. P. (2017). Friction forces position the neural anlage. *Nature Cell Biology*, *19*(4), 306–317. http://doi.org/10.1038/ncb3492

Solnica-Krezel, L. (2005). Conserved patterns of cell movements during vertebrate gastrulation. *Current Biology*, *15*(6), 213–228. http://doi.org/10.1016/j.cub.2005.03.016

Solnica-Krezel, L., & Sepich, D. S. (2012). Gastrulation: Making and Shaping Germ Layers. *Annual Review of Cell and Developmental Biology*, *28*(1), 687–717. http://doi.org/10.1146/annurev-cellbio-092910-154043

Talbot, W. S., Trevarrow, B., Halpern, M. E., Melby, A. E., Farr, G., Postlethwait, J. H., … Kimelman, D. (1995). A homeobox gene essential for zebrafish notochord development. *Nature*, *378*(6553), 150–157. http://doi.org/10.1038/378150a0

Varatharasan, N., Croll, R. P., & Franz-Odendaal, T. (2009). Taste bud development and patterning in sighted and blind morphs of Astyanax mexicanus. *Developmental Dynamics*, *238*(12), 3056–3064. http://doi.org/10.1002/dvdy.22144

Weinberg, E. S., Allende, M. L., Kelly, C. S., Abdelhamid, a, Murakami, T., Andermann, P., … Riggleman, B. (1996). Developmental regulation of zebrafish MyoD in wild-type, no tail and spadetail embryos. *Development (Cambridge, England)*, *122*(1), 271–80. http://doi.org/10.1242/dev.00400

Xu, X., He, Y., Sun, L., Ma, S., & Luo, C. (2014). Maternal Vsx1 plays an essential role in regulating prechordal mesendoderm and forebrain formation in zebrafish. *Developmental Biology*, *394*(2), 264–276. http://doi.org/10.1016/j.ydbio.2014.08.011

Yabe, T., & Takada, S. (2012). Mesogenin causes embryonic mesoderm progenitors to differentiate during development of zebrafish tail somites. *Developmental Biology*, *370*(2), 213–222. http://doi.org/10.1016/J.YDBIO.2012.07.029

Yamamoto, Y., Byerly, M. S., Jackman, W. R., & Jeffery, W. R. (2009). Pleiotropic functions of embryonic sonic hedgehog expression link jaw and taste bud amplification with eye loss during cavefish evolution. *Developmental Biology*, *330*(1), 200–211. http://doi.org/10.1016/j.ydbio.2009.03.003

Yamamoto, Y., & Jeffery, W. R. (2000). Central role for the lens in cave fish eye degeneration. *Science (New York, N.Y.)*, *289*(5479), 631–3. http://doi.org/10.1126/SCIENCE.289.5479.631

Yamamoto, Y., Stock, D. W., & Jeffery, W. R. (2004). Hedgehog signalling controls eye degeneration in blind cavefish, *431*(October). http://doi.org/10.1038/nature02906.1.

Yoshizawa, M., Ashida, G., & Jeffery, W. R. (2012). Parental genetic effects in a cavefish adaptive behavior explain disparity between nuclear and mitochondrial DNA. *Evolution*, *66*(9), 2975–2982. http://doi.org/10.1111/j.1558-5646.2012.01651.x

Yoshizawa, M., Gorički, Š., Soares, D., & Jeffery, W. R. (2010). Evolution of a behavioral shift mediated by superficial neuromasts helps cavefish find food in darkness. *Current Biology*, *20*(18), 1631–1636. http://doi.org/10.1016/j.cub.2010.07.017

Yoshizawa, M., Jeffery, W. R., Netten, S. M. Van, & Mchenry, M. J. (2014). The sensitivity of lateral line receptors and their role in the behavior of Mexican blind cavefish (Astyanax mexicanus), 886–895. http://doi.org/10.1242/jeb.094599

Zhang, J., Houston, D. W., King, M. Lou, Payne, C., Wylie, C., & Heasman, J. (1998). The Role of Maternal VegT in Establishing the Primary Germ Layers in Xenopus Embryos. *Cell*, *94*(4), 515–524. http://doi.org/10.1016/S0092-8674(00)81592-5

Zhang, J., Talbot, W. S., & Schier, A. F. (1998). Positional Cloning Identifies Zebrafish one-eyed pinhead as a Permissive EGF-Related Ligand Required during Gastrulation. *Cell*, *92*(2), 241–251. http://doi.org/10.1016/S0092-8674(00)80918-6

Zhang, T., Yin, C., Qiao, L., Jing, L., Li, H., Xiao, C., … Mo, X. (2014). Stat3-Efemp2a modulates the fibrillar matrix for cohesive movement of prechordal plate progenitors. *Development*, *141*(22), 4332–4342. http://doi.org/10.1242/dev.104885

Figures and legends

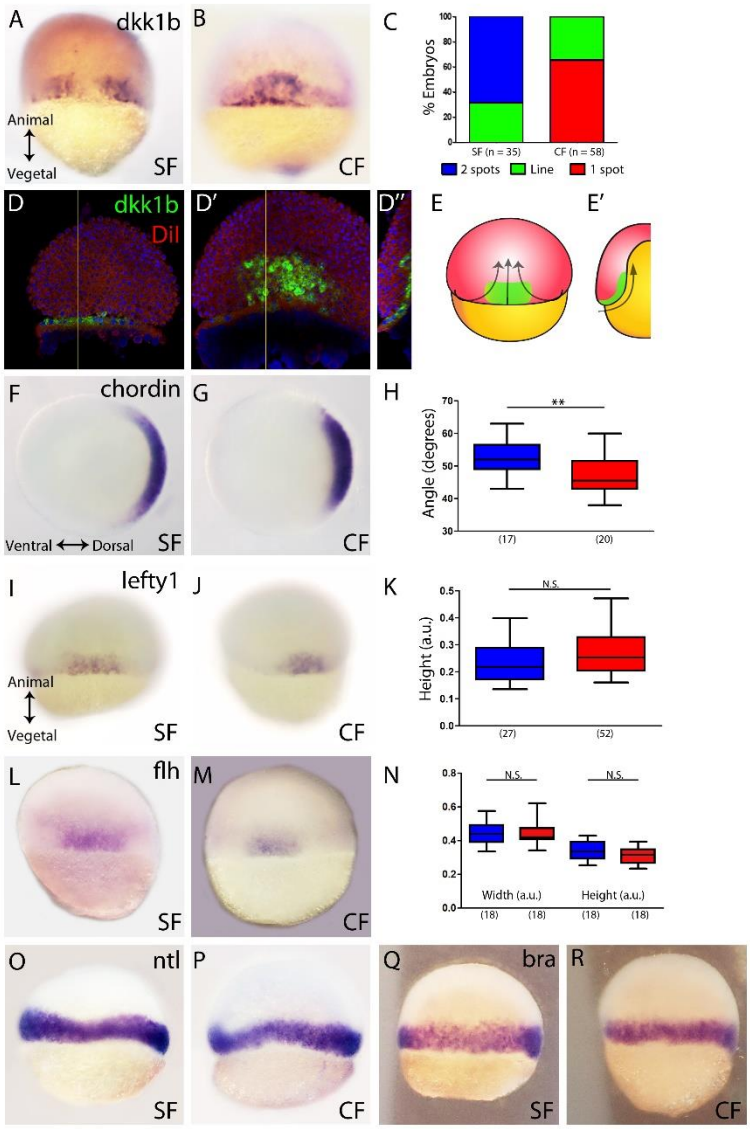

Figure 1.- Expression of genes in the organizer at 50% epiboly in surface fish (SF) and cavefish (CF).

(A-B) Expression of *dkk1b* in surface fish (A) and cavefish (B) in dorsal view. (C) Quantification of the expression patterns observed in each morphotype. The Y-axis indicates the percentage of embryos belonging to each of the categories and the number of embryos analyzed is indicated. “Two spots” (blue) is the pattern observed in A, “1 spot” (red) is the pattern observed in B, and “Line” is an intermediate profile (not shown).

(D-D'') Confocal optical sections of superficial (D) and deep (D') planes and orthogonal section (D'') at the level of the yellow line in D-D' of a cavefish embryo stained with DiI (red) and DAPI (blue) after fluorescent ISH to *dkk1b*. Representation of the cell movements of convergence and internalization (arrows) in a dorsal view (E) and in a section (E'), with the *dkk1b+* cells in green.

(F-G) Expression of *chordin* in surface fish (F) and cavefish (G) in animal view. (H) Quantification of the angle covered *chordin* expression pattern.

(I-J) Expression of *lefty1* in surface fish (I) and cavefish (J) in dorsal view. (K) Quantification of the height for *lefty1* expression.

(L-M) Expression of *flh* in surface fish (L) and cavefish (M) in dorsal view. (N) Quantification of the width (left) and the height (right) of *flh* expression.

(O-P) Expression of *ntl* in surface fish (O) and cavefish (P). (Q-R) Expression of *bra* in surface fish (Q) and cavefish (R).

A, B, D, D', I, J, L, M are dorsal views, animal pole upwards. F, G are animal views, dorsal to the right. Embryos in O, P, Q, R are oriented with the animal pole upwards. Mann-Whitney test were performed. In H, ** = 0.0083.

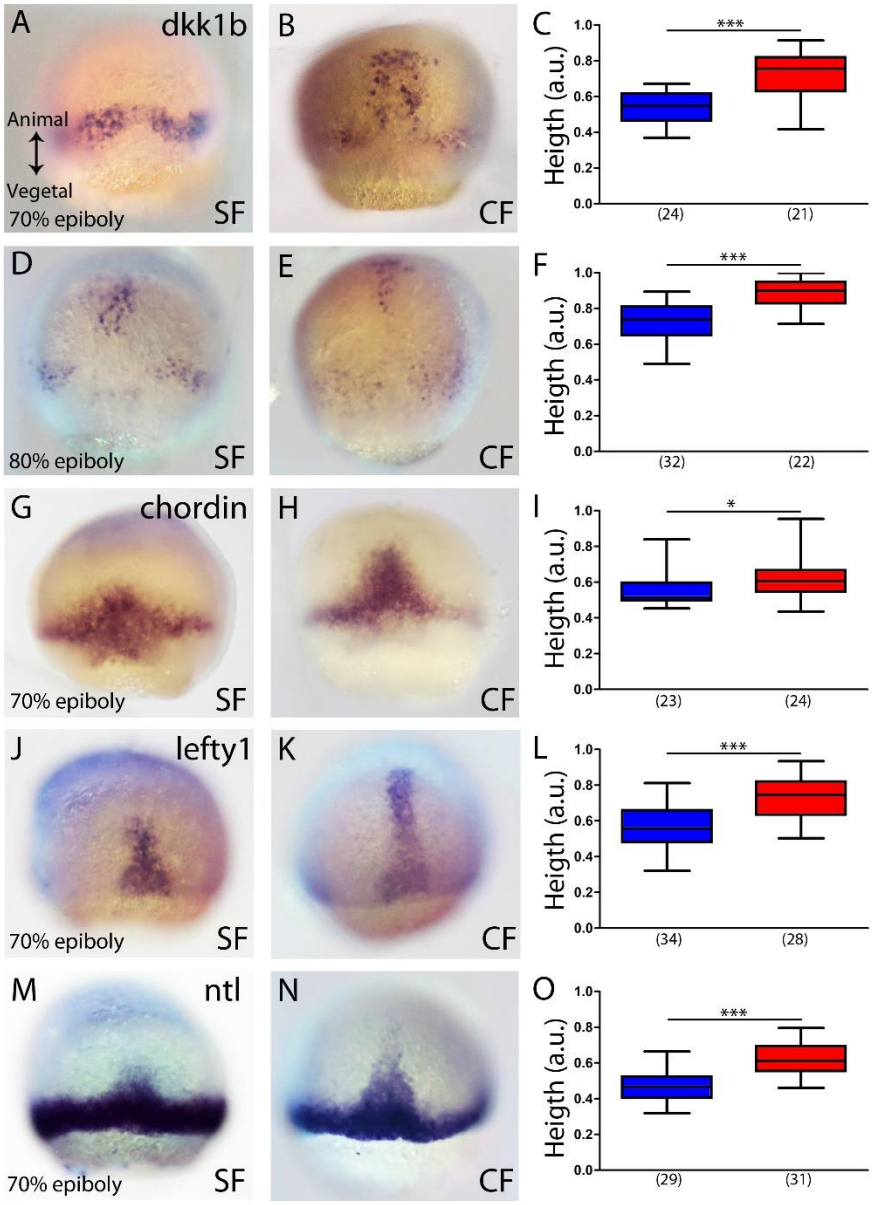

Figure 2.- Expression of axial mesodermal genes during mid-gastrulation in surface fish (SF) and cavefish (CF).

(A-B, D-E) Expression of *dkk1b* in surface fish (A, D) and cavefish (B, E) at 70 and 80 % epiboly (A-B and D-E, respectively). (C, F) Quantification of height in *dkk1b* labeled embryos at 70 and 80% epiboly (C and F, respectively).

(G-H) Expression of *chordin* in surface fish (G) and cavefish (H) at 70% epiboly. (I) Quantification of height in *chordin* labeled embryos at 70% epiboly.

(J-K) Expression of *lefty1* in surface fish (J) and cavefish (K) at 70% epiboly. (L) Quantification of height in *lefty1* labeled embryos at 70% epiboly.

(M-N) Expression of *ntl* in surface fish (M) and cavefish (N) at 70% epiboly. (O) Quantification of height in *ntl* labeled embryos at 70% epiboly.

Embryos in dorsal views, animal pole upwards. Mann-Whitney test were performed. *** < 0.0001, * = 0.0167 (I).

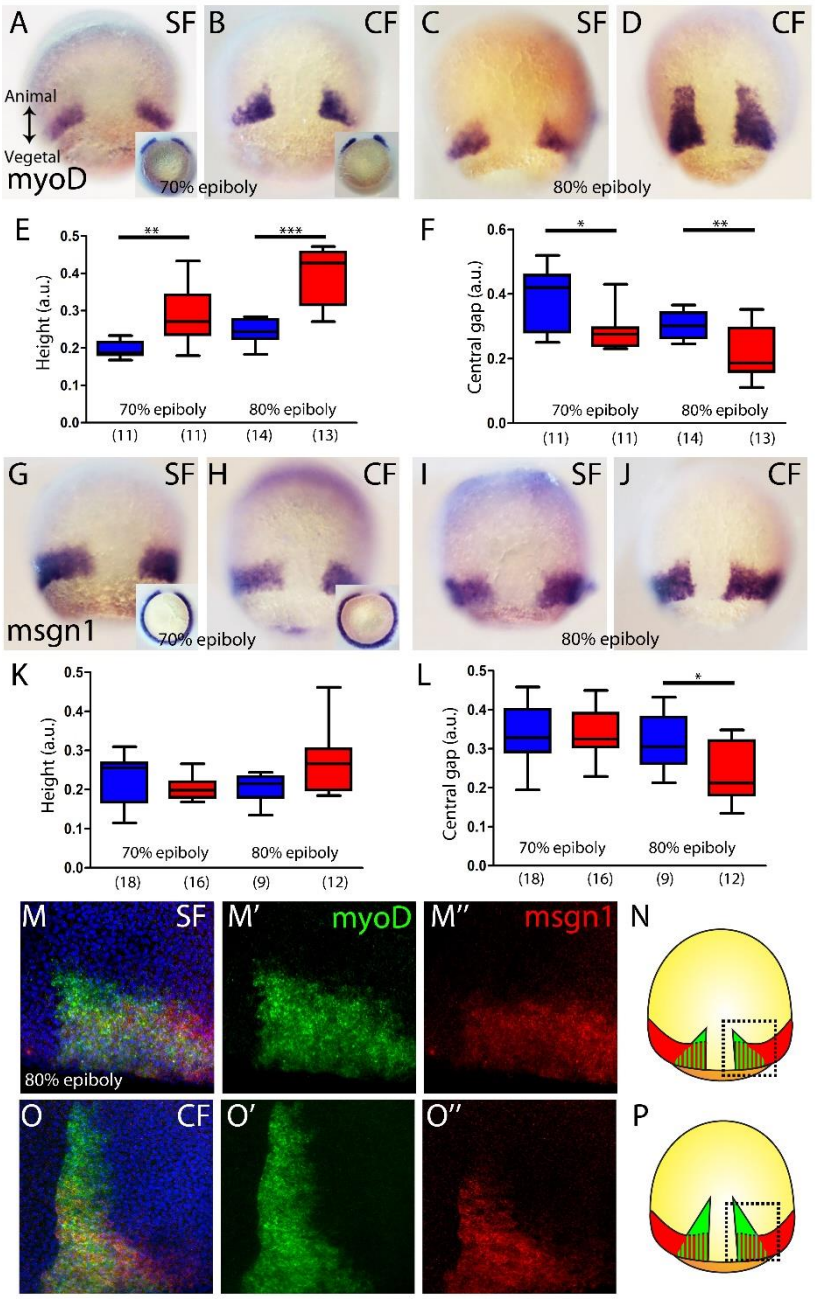

Figure 3.- Internalization of paraxial mesoderm in surface fish (SF) and cavefish (CF).

(A-D) Expression of *myoD* in surface fish (A, C) and cavefish (B, D) at 70 and 80% epiboly (A, B and C, D, respectively) in dorsal views. Insets in A and B show the corresponding embryos in a vegetal view. (E) Quantification of height in *myoD* labeled embryos at 70 and 80% epiboly (left and right, respectively). (F) Quantification of central gap in *myoD* labeled embryos at 70 and 80% epiboly (left and right, respectively).

(G-J) Expression of *msgn1* in surface fish (G, I) and cavefish (H, J) at 70 and 80% epiboly (G, H and I, J, respectively) in dorsal views. Insets in G and H show the corresponding embryos in a vegetal view. (K) Quantification of height in *msgn1* labeled embryos at 70 and 80% epiboly (left and right, respectively). (F) Quantification of central gap in *msgn1* labeled embryos at 70 and 80% epiboly (left and right, respectively).

(M-M'' and O-O''). Confocal projection (20-30 µm) showing the expression of *myoD* (green) and *msgn1* (red) double stained surface fish and cavefish embryos (M-M'' and O-O'', respectively) at 80% epiboly. DAPI was used as a counterstain (blue nuclei). (N and P) representations of surface fish (N) and cavefish (P) embryos, indicating in black dashed lines the regions of interest showed in M and O.

Mann-Whitney test were performed. ** = 0.0025 (E, left), *** <0.0001 (E, right), * = 0.0181 (F, left), ** = 0.0094 (F, right), * = 0.0209 (L, right). Embryos in dorsal view unless otherwise indicated.

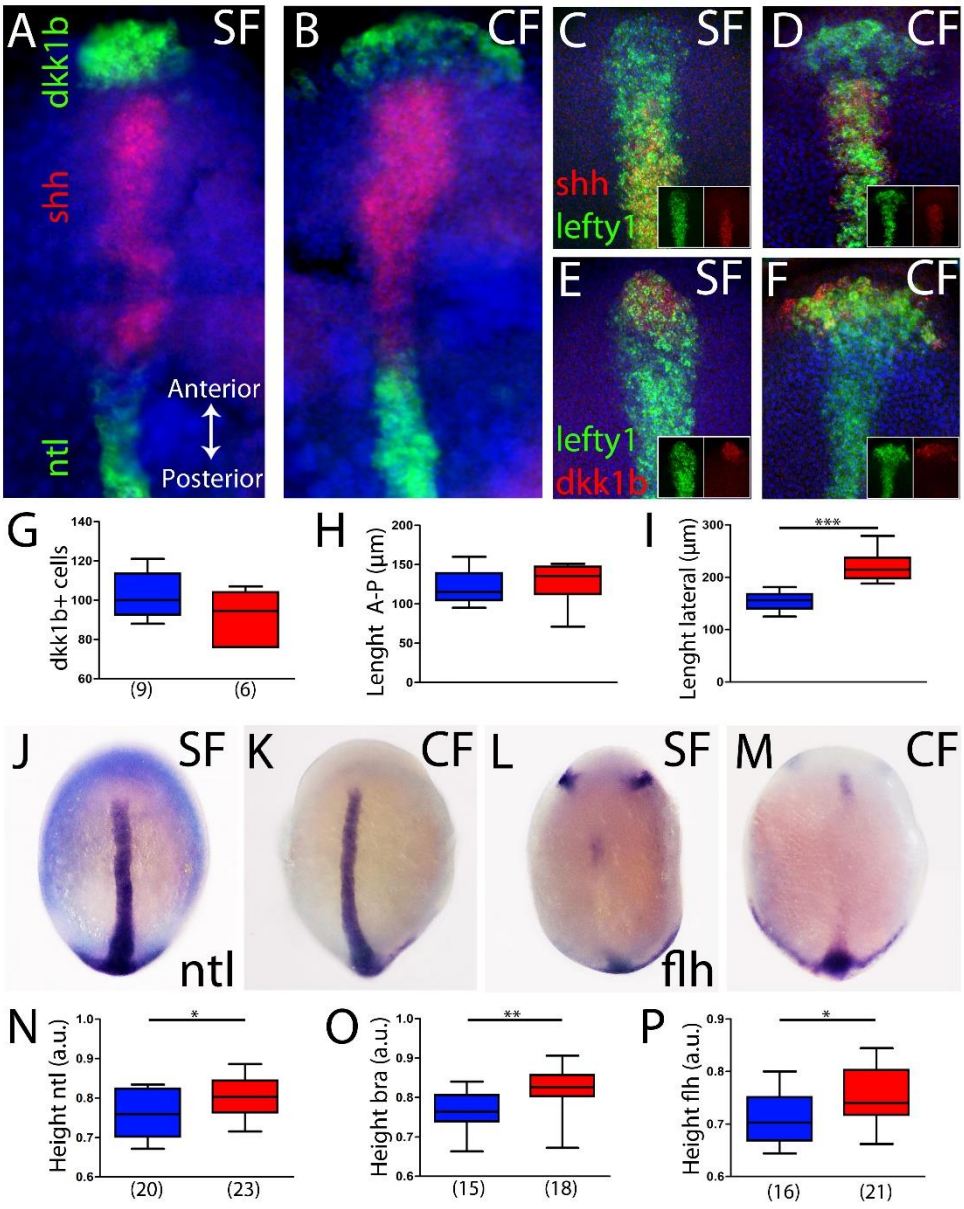

Figure 4.- Axial mesoderm organization in surface fish (SF) and cavefish (CF).

(A-B) Triple ISH to *dkk1b* (green, rostral), *shh* (red, central) and *ntl* (green, posterior) in surface fish (A) and cavefish (B).

(C-D) Confocal projection (20-30 µm) showing the expression of *shh* (red) and *lefty1* (green) in surface fish (C) and cavefish embryos (D). Insets show the split channels.

(E-F) Confocal projection (20-30 µm) showing the expression of *dkk1b* (red) and *lefty1* (green) in surface fish (E) and cavefish embryos (F). Insets show the split channels.

(G) Quantification of cells expressing *dkk1b*. (H) Quantification of the distance between the *dkk1b* expressing cells located in the extremes of the antero-posterior axis. (I) Quantification of the distance between the *dkk1b* expressing cells in in both lateral extremes.

(J-K) Expression of *ntl* in surface fish (J) and cavefish (K). (L-M) Expression of *flh* in surface fish (L) and cavefish (M). (N) Quantification of height in *ntl* labeled embryos. (O) Quantification of height in *bra* labeled embryos. (P) Quantification of height in *flh* labeled embryos.

All embryos are in dorsal view, anterior upwards. Pictures A-F are flat mounted embryos and pictures J-M are whole mount embryos. Mann-Whitney test were performed. *** < 0.0001 (I), * = 0.0396 (N), ** = 0.0012 (O), * = 0.0142 (P).

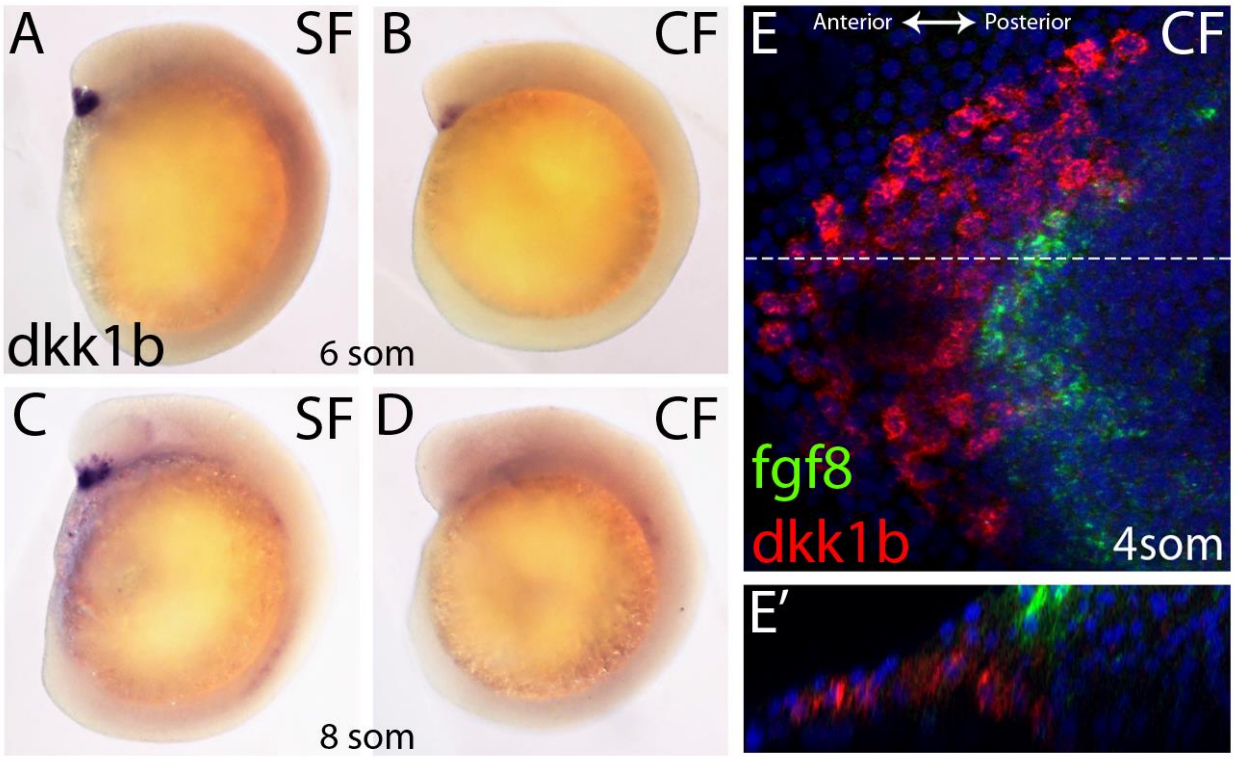

Figure 5.- Off-set of *dkk1b* expression in surface fish (SF) and cavefish (CF).

(A-D) Expression of *dkk1b* at 6 and 8 somite stage (A-B and C-D, respectively) in surface fish (A and C) and cavefish (B and D).

(E-E') Confocal projection (30 µm) after double staining for *dkk1b* (red) and *fgf8* (green) in a cavefish embryo at 4 somite stage (E) and reconstruction at the level indicated in white dashed line (E').

Embryos in lateral view, whole mounted (A-D) and flat dissected mounted embryo (E-E').

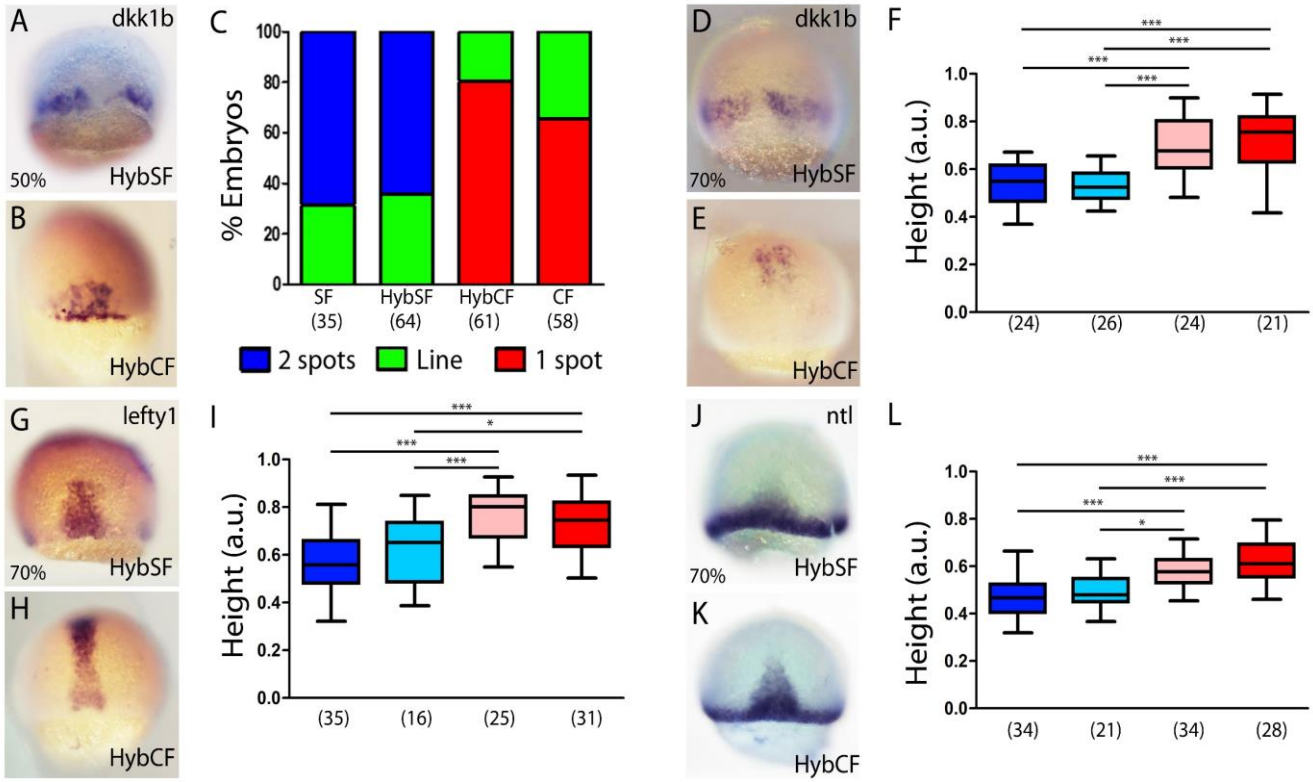

Figure 6.- Maternal effect on gastrulation.

(A-B) Expression of *dkk1b* in HybSF (A) and HybCF (B) at 50% epiboly. (C) Quantification of the expression patterns. The Y-axis indicates the percentage of the total embryos belonging to each of the categories and the numbers of embryos examined are indicated. “Two spots” (blue) is the pattern observed in A, “1 spot” (red) is the pattern observed in B, and “Line” is an intermediate profile (not shown).

(D-E) Expression of *dkk1b* in HybSF (D) and HybCF (E) at 70% epiboly. (F) Quantification of height in *dkk1b* labeled embryos at 70% epiboly.

(G-H) Expression of *lefty1* in HybSF (G) and HybCF (H) at 70% epiboly. (I) Quantification of height in *lefty1* labeled embryos at 70% epiboly.

(J-K) Expression of *ntl* in HybSF (J) and HybCF (K) at 70% epiboly. (L) Quantification of height in *ntl* labeled embryos at 70% epiboly.

All embryos imaged in whole mount, dorsal view, animal pole upwards. ANOVA test with Bonferroni’s post-test were performed in all cases.

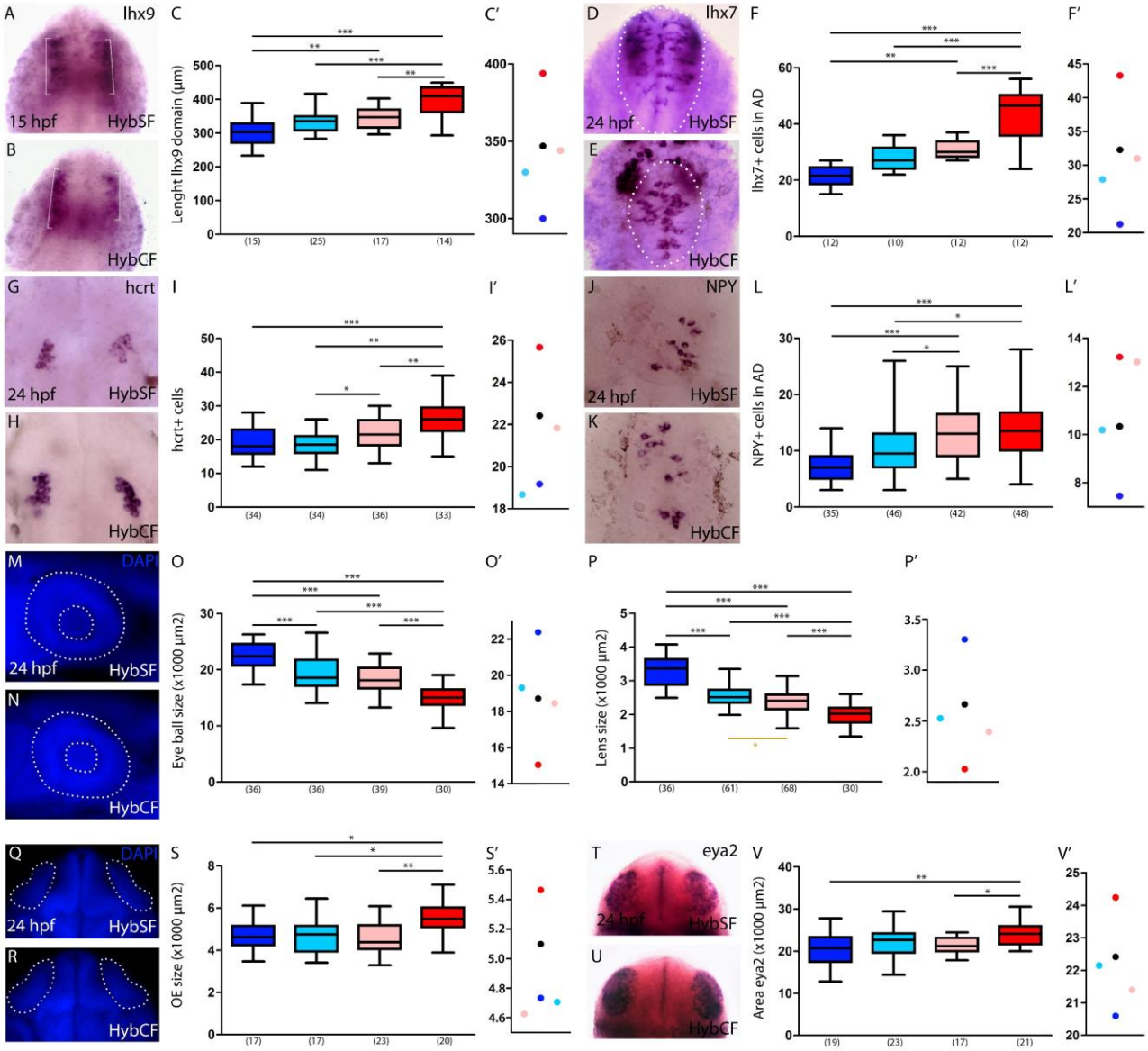

Figure 7.- Maternal effect on later embryogenesis.

(A-B) Expression of *lhx9* in HybSF (A) and HybCF (B) at 15 hpf. (C-C') Quantification of the length of the expression domain in the prospective hypothalamus (white brackets) (C) and the corresponding plot of means distribution (C').

(D-E) Expression of *lhx7* in HybSF (D) and HybCF (E) at 24 hpf. (F-F'). Acroterminal domain indicated in white dashed lines. Quantification of the number of *lhx7* expressing cells in the acroterminal domain (F) and the corresponding plot of means distribution (F').

(G-H) Expression of *hcrt* in HybSF (G) and HybCF (H) at 24 hpf. (I-I') Quantification of the number of hypothalamic *hcrt* expressing cells (I) and the corresponding plot of means distribution (I').

(J-K) Expression of *NPY* in HybSF (J) and HybCF (K) at 24 hpf in the acroterminal domain. (L-L') Quantification of the number of *NPY* expressing cells (L) and the corresponding plot of means distribution (L').

(M-N) DAPI stained HybSF (M) and HybCF (N) embryos at 24 hpf. White dashed lines indicate the contour of the eye ball and the lens (exterior and interior circles, respectively). (O, O', P, P') Quantification of the size of the Eye ball (O) and the size of the lens (P), and their respective plots of means distribution (O' and P').

(Q-R) DAPI stained HybSF (Q) and HybCF (R) embryos at 24 hpf. White dashed lines indicate the contour of the olfactory placodes. (S-S') Quantification of the size of olfactory placodes (S) and the corresponding plot of means distribution (S').

(T-U) Expression of *eya2* in HybSF (T) and HybCF (U) at 24 hpf. (V-V') Quantification of the size of the *eya2* expression domain in the olfactory placodes (V) and the corresponding plot of means distribution (V').

All measurements in this figure were not normalized. A, B, D, E, G, H, J and K are dissected embryos mounted in ventral view, anterior upwards. M, N, Q, R, T and U are whole mounted embryos. M and N are in lateral view, anterior to the left; Q and R are in dorsal view, anterior upwards; T and U are in frontal view, dorsal upwards. ANOVA test with Bonferroni's post-test were performed in all cases.